Available online at www.sciencedirect.com

jmr&t Journal of Materials Research and Technology

journal homepage: www.elsevier.com/locate/jmrt

Original Article

Enhancement of near-infrared response for GaAs-based photocathode with laminated graded-bandgap structure: theory and experiment

Ziheng Wang [a], *Yijun Zhang* [a,*], *Shiman Li* [a], *Shan Li* [a], *Jingjing Zhan* [a], *Yunsheng Qian* [a], *Feng Shi* [b,**], *Hongchang Cheng* [b], *Gangcheng Jiao* [b], *Yugang Zeng* [c]

[a] *School of Electronic and Optical Engineering, Nanjing University of Science and Technology, Nanjing, 210094, China*
[b] *Science and Technology on Low-Light-Level Night Vision Laboratory, Xi'an, 710065, China*
[c] *Changchun Institute of Optics, Fine Mechanics and Physics, Chinese Academy of Sciences, Changchun, 130033, China*

ARTICLE INFO

Article history:
Received 29 March 2022
Accepted 15 May 2022
Available online 21 May 2022

Keywords:
GaAs-based photocathode
Distributed bragg reflection
Near-infrared response
Activation experiment

ABSTRACT

To enhance the quantum efficiency of GaAs-based photocathode in the near-infrared range, a laminated graded-bandgap photocathode structure consisting of a distributed Bragg reflection layer and a graded-bandgap emission layer is proposed. The theoretical optical properties and quantum efficiency of this proposed photocathode are simulated based on the finite-different time-domain method and the one-dimensional continuity equations, respectively. The absorptivity at 1064 nm can be significantly increased for the new-type photocathode because of the secondary absorption caused by the distributed Bragg reflection layer. With the improvement of absorptivity at 1064 nm, the quantum efficiency at specific wavelength is enhanced significantly. The contribution of the DBR structure and built-in electric field to the quantum efficiency is theoretical investigated respectively. According to theoretical structure design, the cathode samples grown by epitaxial technique are prepared to verify the theoretical prediction of quantum efficiency enhancement. After the treatment of surface cleaning and Cs/NF_3 activation, the experimental results show that the minimum reflectivity at 1064 nm is realized, and the quantum efficiency of the sample with proposed structure is ten times than that of the sample without distributed Bragg reflection layer at 1064 nm. This research provides a guidance for the design of novel photocathode structures with enhanced response at special wavelength.

* Corresponding author.
** Corresponding author.
E-mail addresses: zhangyijun423@126.com (Y. Zhang), shfyf@126.com (F. Shi).
https://doi.org/10.1016/j.jmrt.2022.05.099

1. Introduction

Nowadays, the near-infrared (NIR) photodetectors have significance in imaging, environment monitoring, biomedicine, photoelectrochemistry, telecommunications, security check and industrial processing control [1–5]. Since its invention in 1920s, the vacuum photodetector adopting photocathode material is still irreplaceable in certain domains due to the advantages of high-speed response, low thermal noise, single photon detection and large detecting area [6–11]. Because of the excellent absorption characteristics in the NIR wavelength range, InGaAs ternary alloy semiconductor has been widely applied in avalanche diodes, photomultiplier tubes and high-performance image intensifiers operating in the NIR range [12–14]. With the increasing requirements of the performance of photodetectors, the quantum efficiency of InGaAs photocathode at several specific wavelengths still requires to be further improved.

As one of the few photocathodes which has response in the NIR range, the quantum efficiency of non-field-assist InGaAs photocathode at 1064 nm wavelength, as a vital wavelength in practical applications, is still at a low level [15–19]. The photoemission process of InGaAs photocathodes can be described as a three-step model of optical absorption, electron transport to the surface, and escape across the surface barrier into the vacuum [20]. In the absorption process, a large amount of incident light in NIR wavelength range transmit through the emission layer and loss in the substrate, because of the low absorptivity of the InGaAs emission layer in this wavelength range. However, it is impractical to improve the absorption by increasing the thickness of emission layer infinitely, which is limited by the lattice matching problem and electron diffusion length [19,21]. Moreover, in the electron transport process, the problems of lattice mismatching and electron lifetime in InGaAs photocathode also limit the quantum efficiency [18,22].

With the development of semiconductor growth techniques, the varying-composition structure and distributed Bragg reflection (DBR) structure have been introduced into photocathode for quantum efficiency enhancement, which has been proved effectively in previous work [23–32]. Whereas, the improvement of quantum efficiency in the most interesting NIR region, especially at 1064 nm, remains to be studied. In this case, a new laminated GaAs-based photocathode with a varying-composition emission layer and a DBR structure is proposed for realizing the improvement of the quantum efficiency at 1064 nm operating in the reflection mode, which combines the virtues of absorption enhancement, lattice matching and built-in electric field assistance. The reflectivity curve and absorption intensity distribution of this structure is calculated by the finite-different time-domain (FDTD) method. In order to design this new-type photocathode structure reasonably, the theoretical quantum efficiency model of the proposed photocathode is deduced through solving from the one-dimensional continuity equations combined with the three-step model. Accordingly, the relationship among the reflectivity, quantum efficiency and structure parameters is analyzed respectively. Moreover, in order to verify the practicality of the theoretical model, the GaAs-based cathode samples with the proposed laminated graded bandgap structure was grown and then activated, and the experimental quantum efficiency and reflectivity curves are fitted by the deduced theoretical model. Another sample for comparison without DBR structure was also prepared and activated in the same method. Through the comparison of the quantum efficiency and reflectivity, the improvement effect of the new structure design on the NIR response is demonstrated.

2. Structure and theoretical model

The designed structure diagram of the laminated GaAs-based photocathode with DBR layer operating in reflection mode is shown in Fig. 1(a), wherein the emission layer is composed of varying-composition $In_xGa_{1-x}As$. Below the emission layer, the DBR layer formed by two alternate lattice matching materials

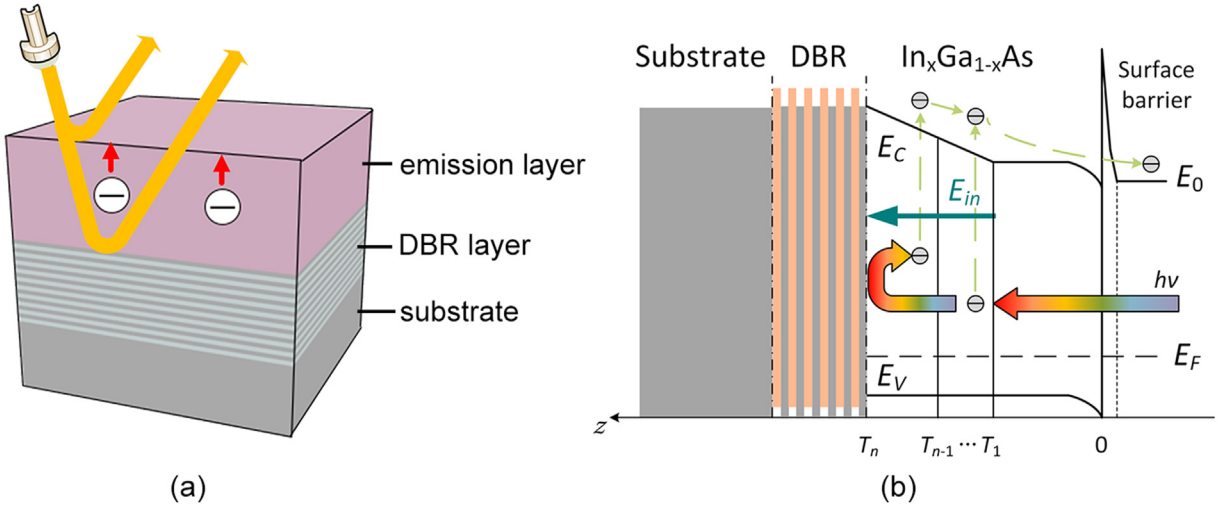

Fig. 1 – (a) Designed structure diagram and (b) energy band structure of the proposed laminated GaAs-based photocathode. E_C is the minimum of conduction-band, E_V is the maximum of valence-band, E_F is the Fermi level, E_0 is the vacuum level and E_{in} is the built-in electric field.

is grown on the high quality GaAs substrate. The DBR layer has the function of reflecting incident light at specific wavelength, which will be described in detail below. The incident light at specific wavelength passes through the emission layer and is reflected by the DBR layer back to the emission layer for forming secondary absorption. Figure 1(b) shows the energy band structure of the proposed laminated GaAs-based photocathode. The $In_xGa_{1-x}As$ emission layer is divided into a graded bandgap region and a uniform composition region. The In composition in the graded bandgap region gradually increases from bulk to the surface for generating built-in electric field. The uniform composition region without built-in electric field is grown above the graded bandgap region to improve the absorption in NIR wavelength range. Through the varying-composition growth, the lattice mismatching problem can be improved and the emission layer with higher In composition can be obtained [33]. It can be seen that the downward conduction-band in emission layer is arising from the increase of In composition, which generates a built-in electric field in graded bandgap region in the direction from surface to bulk. The photoelectrons generated in the graded bandgap region drift toward the uniform composition region with the assist of built-in electric. The boundary materials in DBR layer are designed to have a wider bandgap than that of the emission layer. In this case, the DBR layer also acts as an electron blocking layer, which has the function of preventing reverse recombination of excited electron. As one of the typical combination of superlattice materials, the valence band maximum of the GaAs is lower than that of the AlAs, which causes the asymmetric structure of the energy band in the DBR layer, as shown in Fig. 1(b).

Because of the large absorption depth of the light in the NIR wavelength range, the quantum efficiency is limited for the conventional InGaAs photocathode. In order to improve the absorption situation at 1064 nm, a DBR layer is introduced between the emission layer and the substrate, as shown in Fig. 1(a). Through the specific structural design of DBR layer, the total reflection at the specific wavelength can be realized. In this case, the original light in the direction toward the substrate would be reflected back to the emitting layer for the secondary absorption, which improves the absorptivity of the emission layer without changing the thickness. To realize the total reflection at the 1064 nm wavelength, the parameters of the DBR layer need to satisfy the following equations

$$\frac{2\pi}{\lambda}n_L d_L = \frac{\pi}{2} \tag{1}$$

$$\frac{2\pi}{\lambda}n_H d_H = \frac{\pi}{2} \tag{2}$$

where n_L and n_H are the refractive index of the materials in the DBR layer respectively, and $n_H > n_L$, d_L and d_H are the thickness of this two materials in each alternation period, and λ is the target wavelength. In this work, the target wavelength is set as 1064 nm. The reflectivity at 1064 nm is determined by the number of alternating periods of the two materials.

For computability, the emission layer is divided into n sublayers. The sublayer 1 is the uniform composition region and the graded bandgap region is composed by the sublayer 2 to n. As shown in Fig. 1(b), the built-in electric field E_{in} is generated in the graded bandgap region, and the intensity of E_{in} can be calculated by the following formula:

$$E_{\mathrm{in}} = \begin{cases} \dfrac{E_{gn} - E_{g1}}{T_n - T_1}, & z \geq T_1 \\ 0\ , & z < T_1 \end{cases} \tag{3}$$

where E_{gn} and E_{g1} are the bandgap of the innermost sublayer and the outmost sublayer in the graded bandgap region, T_n is the total thickness of the emission layer, and T_1 is the thickness of uniform composition region.

According to Spicer's three-step model of photoemission [20], the quantum efficiency of this laminated GaAs-based photocathode can be deduced from one-dimensional continuity equation [34], which is given by

$$D_{\mathrm{i}}\frac{d^2 n_{\mathrm{i}}(z)}{dz^2} + \mu_{\mathrm{i}}|E_{\mathrm{in}}|\frac{dn_{\mathrm{i}}(z)}{dz} - \frac{n_{\mathrm{i}}(z)}{\tau_{\mathrm{i}}} + g_{\mathrm{i}}(z) = 0, \quad \mathrm{i} = 1, 2, 3\ldots, n \tag{4}$$

For the photocathode operating in the reflection mode, the generation rate of photoelectrons $g_i(z)$ can be expressed as follows

$$g_{\mathrm{i}}(z) = \begin{cases} (1-R_{h\upsilon})I_0\alpha_{h\upsilon 1}\exp(-\alpha_{h\upsilon 1}z), & \mathrm{i}=1 \\ (1-R_{h\upsilon})I_0\alpha_{h\upsilon i}\left[\prod_{m=1}^{i-1}\exp(-\alpha_{h\upsilon m}d_m)\right]\exp[-\alpha_{h\upsilon i}(z-T_{i-1})], & \mathrm{i}\neq 1 \end{cases} \tag{5}$$

In Eqs. (4) and (5), $R_{h\upsilon}$ is the reflectivity of incident surface, I_0 is the intensity of incident light, $\alpha_{h\upsilon}$ is the absorption coefficient, d_m is the thickness of each sublayer, T_i is the position of each sublayer along the z axis, D_i is the electron diffusion coefficient, μ_i is electron mobility, $n_i(z)$ is the electron concentration, τ_i is the lifetime of electron, and the subscript i values from 1 to n, corresponding to each sublayer with different In composition.

To solve Eq. (4), the boundary conditions of each interface between sublayers are required, and the equations are given as follows:

when $i = 2,\ldots n\text{-}1$,

$$\left[D_{\mathrm{i}}\frac{dn_{\mathrm{i}}(z)}{dz} + \mu_{\mathrm{i}}|E_{\mathrm{in}}|n_{\mathrm{i}}(z)\right]|_{z=T_{\mathrm{i}}} = [-S_{v\mathrm{i}}n_{\mathrm{i}}(z) + S_{v\mathrm{i}}n_{\mathrm{i}+1}(z)]|_{z=T_{\mathrm{i}}} \tag{6}$$

$$\left[D_{\mathrm{i}}\frac{dn_{\mathrm{i}}(z)}{dz} + \mu_{\mathrm{i}}|E_{\mathrm{in}}|n_{\mathrm{i}}(z)\right]|_{z=T_{\mathrm{i}-1}} = S_{v(\mathrm{i}-1)}n_{\mathrm{i}}(z)|_{z=T_{\mathrm{i}-1}} \tag{7}$$

when $i = n$, the boundary condition becomes

$$\left[D_{\mathrm{i}}\frac{dn_{\mathrm{i}}(z)}{dz} + \mu_{\mathrm{i}}|E|n_{\mathrm{i}}(z)\right]|_{z=T_n} = -S_{v\mathrm{i}}n_{\mathrm{i}}(z)|_{z=T_n} \tag{8}$$

$$\left[D_{\mathrm{i}}\frac{dn_{\mathrm{i}}(z)}{dz} + \mu_{\mathrm{i}}|E_{\mathrm{in}}|n_{\mathrm{i}}(z)\right]|_{z=T_{n-1}} = S_{v(n-1)}n_{\mathrm{i}}(z)|_{z=T_{n-1}} \tag{9}$$

when $i = 1$, the boundary condition becomes

$$\left[D_1\frac{dn_1(z)}{dz}\right]|_{z=T_1} = [-S_{v1}n_1(z) + S_{v1}n_2(z)]|_{z=T_1} \tag{10}$$

$$n(0) = 0 \tag{11}$$

where S_v is the interface recombination velocity, and S_{vi} is the recombination velocity at the interface between sublayer i and sublayer $i+1$. As for the varying-composition $In_xGa_{1-x}As$ emission layer, the band gap, electron mobility, electron diffusion coefficient all depend on the In composition x, and the relationship expressions are given by [35].

$$E_g(x) = 0.36 + 0.63(1-x) + 0.43(1-x)^2 \ \ (eV) \tag{12}$$

$$\mu(x) = 40 - 80.7(1-x) + 49.2(1-x)^2 \ \ \left(cm^2V^{-1}s^{-1}\right) \tag{13}$$

$$D(x) = \left[10 - 20.2(1-x) + 12.3(1-x)^2\right] \times 100 \ \ \left(cm^2s^{-1}\right) \tag{14}$$

Through substituting the generation rate of photoelectrons and the boundary conditions into Eq. (4), the general solution of the one-dimensional continuity equation can be obtained. Because of the existence of DBR layer, the light absorbing process in the emission layer is divided into front-side incident absorption and secondary absorption. In calculation, the contribution of these two absorptions to quantum efficiency is calculated separately. The quantum efficiency $Y_{front,}$ arising from the front-side incidence of photons, can be calculated via the electron concentration distribution in steady state, which is given by [36].

$$Y_{front}(h\nu) = P_{h\nu}D_1\frac{dn_1(z)}{dz}\Big|_{z=0}\Big/ I_0 \tag{15}$$

where the surface electron escape probability $P_{h\nu}$ is given as [37].

$$P_{h\nu} = P_0 \cdot \exp\left[K \cdot \left(\frac{1}{1.14} - \frac{1}{1240/\lambda}\right)\right] \tag{16}$$

where P_0 is the escape probability of an electron excited by an incident photon of 1.14 eV, K is the surface potential barrier factor. Because of the existence of the DBR layer, the incident light is reflected at the interface of DBR and the emission layer, which causes the reversed secondary absorption in the emission layer. Hence, the absorption process of the incident light in the emission layer can be decomposed into the sum of the absorption of front-side incident light and back-side reflected light with special incident luminous intensity distribution. Hence, the quantum efficiency of the new-type photocathode structure can be seen as the sum of the quantum efficiency produced by front-side incident light and back-side reflected light. In this back-side reflected condition, the photoelectrons generation rate in the $In_xGa_{1-x}As$ emission layer is expressed as

$$g_i'(z) = \begin{cases} (1-R_{h\nu})I_1\alpha_{h\nu n}\exp[-\alpha_{h\nu n}(T_n - z),] & i = n \\ (1-R_{h\nu})I_1\alpha_{h\nu i}\left[\prod_{m=i+1}^{n}\exp(-\alpha_{h\nu m}d_m)\right]\exp[-\alpha_{h\nu i}(T_{i-1} - z)], & i \neq n \end{cases} \tag{17}$$

where the back-side reflected light intensity I_1 can be obtained as follows

$$I_1 = I_0 \cdot T_{emi} \cdot R_{DBR} \tag{18}$$

where R_{DBR} is the reflectivity spectrum of the DBR layer, and T_{emi} is the transmissivity of emission layer. Hence, the quantum efficiency Y_{back} produced by the back-side reflected light is given as

$$Y_{back}(h\nu) = P_0D_1\frac{dn_1'(z)}{dz}\Big|_{z=0}\Big/ I_0 \tag{19}$$

Eventually, the total quantum efficiency Y_{total} of the proposed GaAs-based photocathode can be calculated as

$$Y_{total} = Y_{front} + Y_{back} \tag{20}$$

3. Theoretical simulation

By combination of the DBR structure and the varying-composition structure, the quantum efficiency of the new-type GaAs-based photocathode is expected to be enhanced at 1064 nm, which can be attributed to the improvement of absorptivity, better lattice matching and the built-in electric field. To confirm this conjecture, the relationship between the reflectivity and the structural parameters need to be studied firstly for the optimal optical properties. Afterwards, the reflectivity and the absorptivity curves of the photocathode with the suitable structural design can be simulated. Eventually, the quantum efficiency curves of the proposed photocathode and the conventional structure can be simulated and compared for investigating the improvement at 1064 nm.

To simulate the optical properties and the quantum efficiency of the proposed structure, the structural parameters are assumed as follows: the $In_xGa_{1-x}As$ emission layer is divided into 5 sublayers, and the In composition values of each sublayer are 0.05, 0.10, 0.15, 0.20 and 0.20, respectively, from bulk to surface. The thicknesses of these sublayers are 0.1 μm, 0.1 μm, 0.1 μm, 0.1 μm and 0.7 μm, from bulk to surface. The emission layer is divided into uniform composition region and graded bandgap region. The $In_{0.2}Ga_{0.8}As$ sublayer with 0.7 μm thickness is seen as a uniform composition region in the emission layer, while the graded bandgap region consists of the other sublayers with different In composition. In simulation, it is assumed that the bandgap grades linearly in the graded bandgap region. Further, the intensity of the built-in electric field is uniform in the graded bandgap region, and it is assumed that there is no built-in electric field in the uniform composition region. The refractive index and extinction coefficient of GaAs and AlAs are referred to Ref. [38], while the refractive index and extinction coefficient of $In_xGa_{1-x}As$ are referred to Ref. [39]. According to the Eqs. (1) and (2), the optimal thicknesses of the GaAs and AlAs sublayer in the DBR structure are 76 nm and 90 nm, respectively, to reach the maximum reflectivity at 1064 nm. The quantity cycle of the

DBR layers is set to 10 times. The varying-composition $In_xGa_{1-x}As$ photocathode structure without DBR layer is also simulated for comparison. The emission layers of the contrast object have the same structural design as that of the proposed structure.

The FDTD method is utilized to theoretically calculate the reflectivity spectrum at different interface. In the process of simulation, the emission layer is illuminated by a plane wave beam as light source starting from vacuum space, the light beam is perpendicularly incident onto the surface of emission layer. In this case, the emission layer structure can be treated as one-dimensional model in FDTD calculation along the z-axis, and the emission layer can be regarded as a periodic structure in the y-axis direction. The virtual light power monitors are placed above the light source and the bottom of the DBR layer to obtain the surface reflectivity spectrum $R_{h\upsilon}$ and the transmissivity of the photocathode. Besides, the transmissivity T_{emi} of the emission layer is obtained by the monitor placed at the interface between the emission layer and the DBR layer, while the reflectivity R_{DBR} of the DBR layer is obtained by the light source placing in the $In_{0.05}G_{0.95}As$ sublayer and the monitor placed behind the light source. The absorption coefficient of the $In_xGa_{1-x}As$ material is obtain by Ref. [39].

According to the incident light path, the surface reflectivity of the photocathode is determined by the structure of the DBR layer and emission layer together. By studying the surface reflectivity under different photocathode structures, the structure can be optimized to maximize light absorption at 1064 nm. To achieve the maximum absorptivity of the proposed photocathode at 1064 nm, the surface reflectivity should reach the minimum value at 1064 nm and the absorptivity of the emission layer should reach the maximum value at 1064 nm at the same time. The surface reflectivity curves of different thicknesses of the emission layer is simulated and shown in Fig. 2(a). It can be found that the minimum of the reflectivity curves shifts with the thickness of emission layer changing. As can be seen from Fig. 2(a), when the thickness of the emission layer is 1.1 μm, the requirements is satisfied at 1064 nm and the surface reflectivity at this wavelength reaches the minimum. In addition, the optical properties of the structure with and without DBR layer are simulated for comparison, as shown in Fig. 2(b). The *R*, *T* and *A* in this diagram represent the reflectivity, transmissivity and absorptivity of the whole photocathode respectively. It is noted that the absorptivity of photocathode with DBR structure at 980 nm and 1064 nm is obviously enhanced because of the contribution of the secondary absorption of the back-side reflected light caused by the DBR layer.

According to the above discussion, the thickness of the emission layer of the new proposed GaAs-based photocathode should be set as 1.1 μm to maximize the absorptivity at 1064 nm. Considering the $In_{0.2}Ga_{0.8}As$ sublayer has the highest absorption ability at 1064 nm, the thicknesses of each sublayer in the emission layer are set as 0.1 μm, 0.1 μm, 0.1 μm, 0.1 μm and 0.7 μm, from the bulk to the emitting surface. The other parameters utilized in the simulations are listed in Table 1 in detail. By combining these parameters, the quantum efficiency of the laminated GaAs-based photocathode can be obtained by solving Eq. (4). As shown in Fig. 3(a), the quantum efficiency curves of the proposed photocathode structure and the structures for comparison are exhibited. The solid line represents the quantum efficiency curve of the proposed structure and the secondary absorption is considered in calculation, and the dash line represents the quantum efficiency curve of the same structure but the secondary absorption is ignored for comparison. Meanwhile, the quantum efficiency curve of the conventional reflection-mode graded-bandgap $In_xGa_{1-x}As$ photocathode structure without DBR layer is represented by the dot line. The dot dash line represents the quantum efficiency curve of the proposed structure, but the built-in electric field is ignored in the calculation to exhibit the effect of built-in electric field on quantum efficiency. The purpose of ignoring secondary absorption and intensity of electric filed in calculation is to investigate how these structural parameters contribute to the quantum efficiency, but

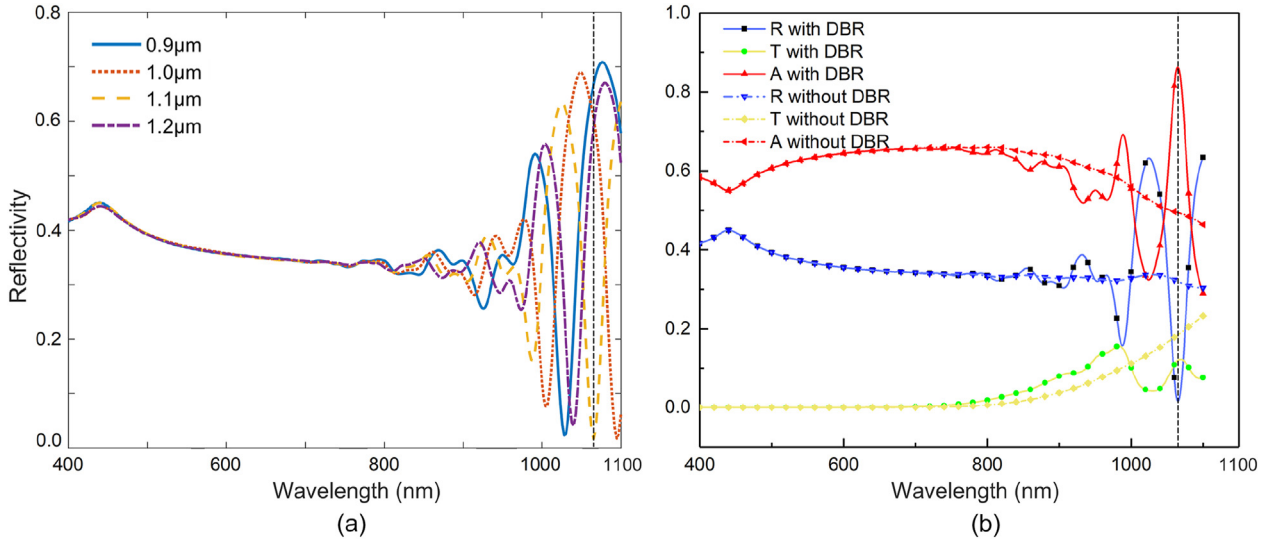

Fig. 2 – (a) Simulated reflectivity curves with different thicknesses of emission layer and (b) simulated reflectivity, transmissivity and absorptivity curves of the photocathode structure with and without DBR layer.

Table 1 – Parameters used in the simulation of quantum efficiency curves.

Parameter	Value	Description
S_{v5}	10^5 cm/s	Electron recombination at the interface between GaAs and $In_{0.05}Ga_{0.95}As$ sublayer
$S_{v2\sim4}$	10^4 cm/s	Electron recombination at $In_xGa_{1-x}As$ interior interfaces
S_{v1}	10^3 cm/s	Electron recombination at the interface between graded bandgap region and uniform composition region
P_0	0.17 (Ref. [21])	Surface electron escape probability
L_5	1.2 μm (Ref. [19])	Electron diffusion length of $In_{0.05}Ga_{0.95}As$
L_4	1.1 μm (Ref. [19])	Electron diffusion length of $In_{0.10}Ga_{0.90}As$
L_3	0.9 μm (Ref. [19])	Electron diffusion length of $In_{0.15}Ga_{0.85}As$
L_1, L_2	0.8 μm (Ref. [19])	Electron diffusion length of $In_{0.20}Ga_{0.80}As$

these structure models do not exist in practice. In the range from 950 nm to 1100 nm, it can be found that the quantum efficiency denoted by the solid line is obviously higher than that denoted by the dash line, and the difference of these two quantum efficiency curves is caused by the secondary absorption of the back-side reflected light from DBR layer. When the wavelength of incident light low than 950 nm, the effect of the secondary absorption on quantum efficiency is not obvious. For the incident light in the wavelength from 400 nm to 950 nm, the emission layer is thick enough to absorb the light in this wavelength range. Besides, due of the total reflection effect of DBR layer at 1064 nm, the improvement of the secondary absorption on the quantum efficiency is most obvious at 1064 nm. It is clear to see that the improvement effect of the built-in electric field is weak in short wavelength range, which is because the thick uniform composition region prevent the light in this range entering the built-in electric region. Without the assistance of DBR layer, the quantum efficiency of the conventional structure without DBR layer is significantly lower than that of the proposed structure. Considering the emission layers of these different photocathode structure are identical, the difference of quantum efficiency is attributed to the improved absorptivity at 1064 nm by DBR layer. For the proposed structure, the introduction of the DBR layer causes the secondary absorption in the emission layer and enhances the quantum efficiency at 1064 nm effectively. The absorption intensity distribution diagrams of the photocathode structure with and without DBR layer at 1064 nm are shown in Fig. 3(b). It can be clearly seen that the absorption intensity of the emission layer of the proposed structure is significantly higher than that of the structure without DBR layer, which agrees well with the simulated results of absorptivity curves shown in Fig.2(b).

4. Experiment and analysis

To verify the quantum efficiency models of the proposed laminated GaAs-based photocathode and the effect of the enhancement of quantum efficiency at 1064 nm, the photocathode sample with the designed structure was prepared. As shown in Fig. 4(a), the DBR layer and the emission layer were grown successively on the high-quality GaAs (100)-oriented substrates with a low dislocation density by the metal–organic chemical vapor deposition (MOCVD) technique. The DBR layer is composed of the p-type AlAs sublayers and p-type GaAs

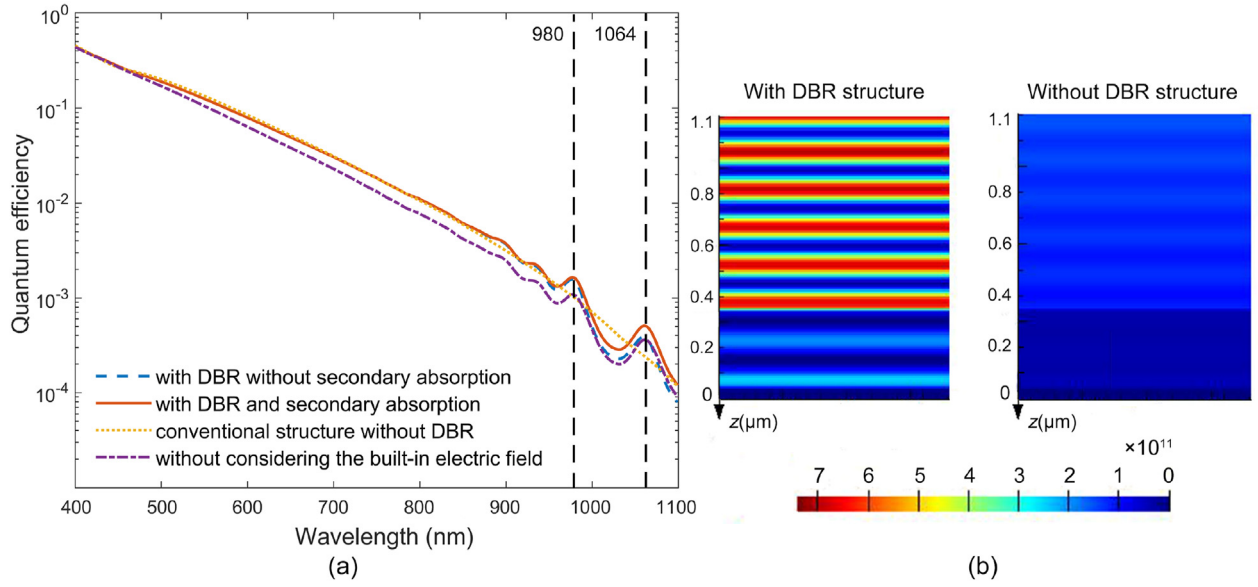

Fig. 3 – (a) Quantum efficiency curves of the photocathode with different structures and (b) optical absorption intensity distribution of the structure with and without DBR structure at 1064 nm.

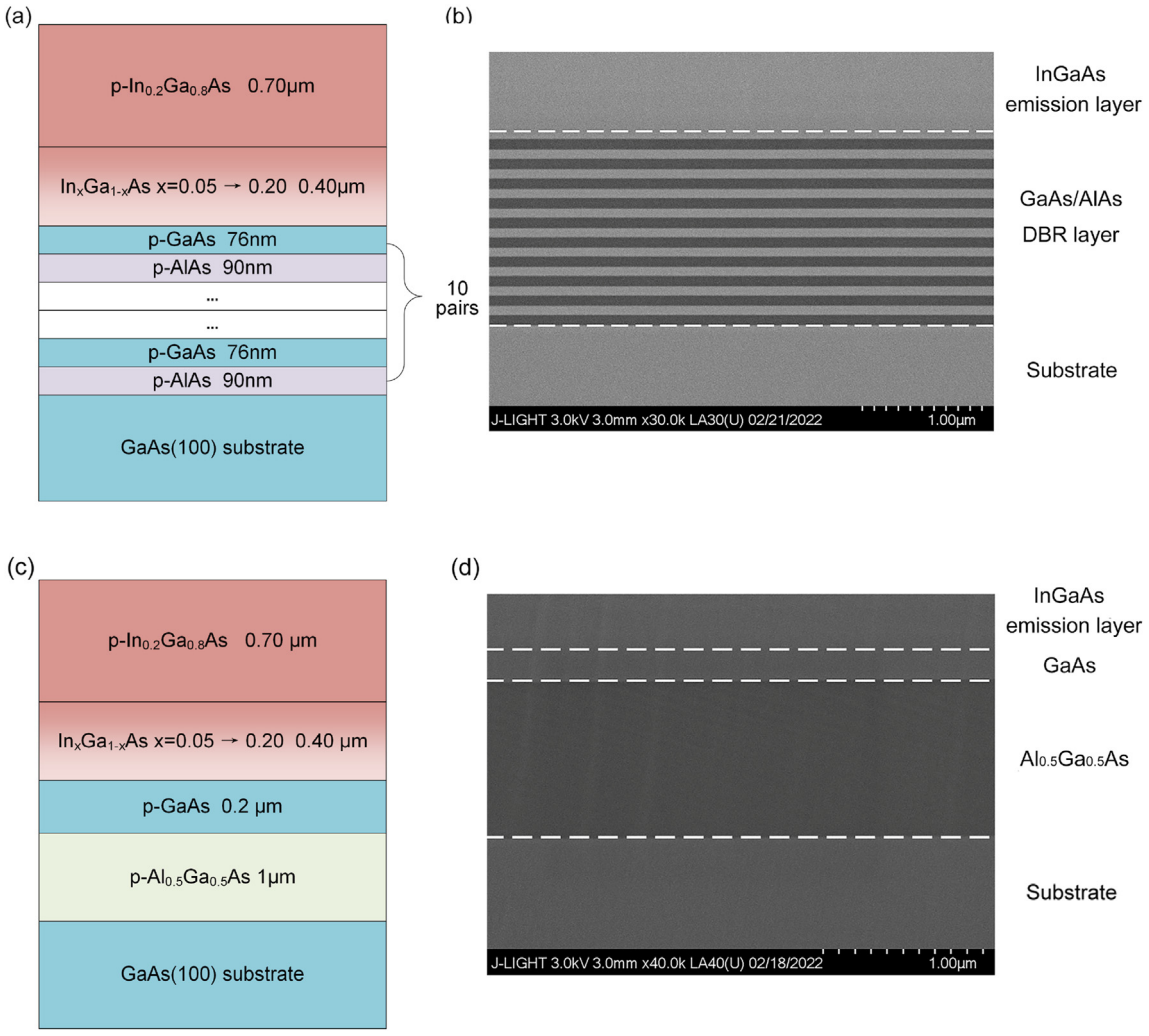

Fig. 4 – (a) Structure diagram and (b) cross section SEM image of the grown laminated GaAs-based cathode sample with DBR structure. (c) Structure diagram and (d) cross section SEM image of the GaAs-based cathode sample without DBR structure.

sublayers, the thickness of each GaAs sublayer and AlAs sublayer is 76 nm and 90 nm, respectively. The doping concentration of the sublayers in the DBR layer is $1 \times 10^{19} cm^{-3}$. In this feasibility study, the pair of alternation layers of the DBR layer is set as 10 for cost reduction. Considering the photo energy loss in the DBR layer, the outermost sublayer is designed as GaAs sublayer with higher refractive index. The p-type emission layer is composed of a graded bandgap region and a uniform composition region. Wherein, the thickness of the graded bandgap region is 0.4 μm and the In composition increases linearly from 0.05 to 0.20. Above the graded bandgap region, the thickness of the uniform composition region is 0.7 μm and the In composition is 0.20. The doping concentration of the emission layer is $1 \times 10^{19} cm^{-3}$. In the growth process, the metal-organic compounds trimethylgallium (TMGa), trimethylalumium (TMAl) and trimethylindium (TMIn) were used as the group III sources, while the arsine (AsH_3) was used as the group V source and diethylzinc (DEZn) was utilized as the dopant source. The high-purity H_2 was used as the carrier gas. The growth temperature of the InGaAs emission layer and the AlAs/GaAs alternating layers was 620 °C and 660 °C, respectively. The epitaxial growth rate was 1 μm/h under the pressure of reaction chamber of 100 mbar and the V/III ratio was kept at about 50. The section image photographed by the scanning electron microscope (SEM) of the proposed structure is shown in Fig. 4(b), which exhibits the internal structure of the sample clearly and shows that the actual structure meets the design requirement. In order to experimentally verify the superiority of the proposed structure, another sample of graded-bandgap $In_xGa_{1-x}As$ photocathode without DBR layer was prepared for comparison. The material growth structure diagram of the photocathode is shown in Fig. 4(c) and the section image photographed by the SEM of the sample without DBR is shown in Fig. 4(d).

Before the activation, a two-step surface cleaning procedure including a surface chemical cleaning process and a heat treatment process in vacuum were performed for cleaning the surface contamination, such as oxides and carbon residues. Firstly, the degreasing cleaning treatment, and etching treatment in hydrochloric acid and isopropanol mixed solution were operated on the sample in sequence. After that, the sample was heated in the vacuum chamber at 600 °C to achieve the atomic-level cleaning surface. During the cesium (Cs) and nitrogen trifluoride (NF_3) activation, the improved co-

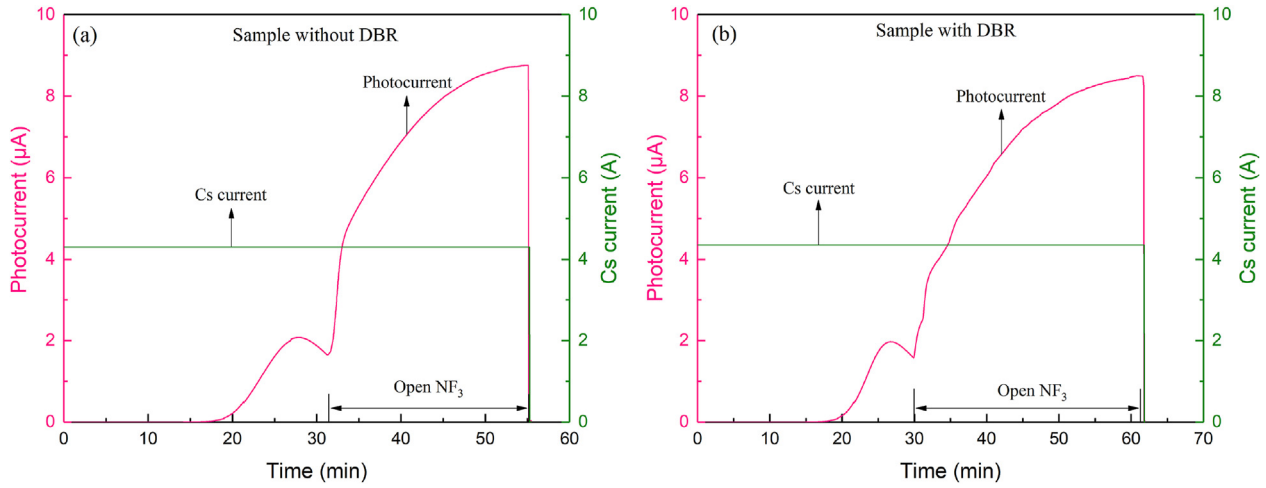

Fig. 5 – Time dependence of the photocurrent of (a) sample without DBR and (b) sample with DBR under tungsten lamp excitation.

deposition activation technique was utilized in an ultrahigh vacuum chamber with base pressure better than 1×10^{-7} Pa, in which Cs source was kept continuously and NF_3 source was introduced when the photocurrent of the Cs peak reached 80%. Finally, the quantum efficiency curve was measured in situ by an online quantum efficiency measurement system. The comparative sample was cleaned and activated by the same technology as the sample with DBR structure. The photocurrents and related parameters during the activation process of these samples are shown in Fig. 5 in detail.

The experimental reflectivity curve of the cathode sample surface was measured by the spectrophotometer, and is exhibited in Fig. 6(a). The measured results indicate that the designed structure achieves the minimum of absorptivity at 1064 nm through DBR layer. The peaks and valleys positions of the fitted curve represented by solid line match well with those of the experimental curve represented by the dash line, and the minimum reflectivity appears at 1064 nm in the experimental curve, which verifies the results of the theoretical optical properties. The experiment and theoretical quantum efficiency curves are shown in Fig. 6(b). It is noted that there are two peak in the experimental quantum efficiency at the 980 nm and 1064 nm, which has been predicted in the aforementioned theoretical simulation in Fig. 3(a). As shown in Fig. 6(b), the quantum efficiency curves begin to oscillate from 900 nm wavelength, which indicates that the effect of the DBR layer gradually appears with the increase of wavelength. By a fit of the experimental quantum efficiency curve via the deduced theoretical model, the fitted parameters in the model can be obtained, which is listed in Table 2. It is found that the surface barrier factor is still large resulting in the lower surface electron escape probability, which should be related to the difficulty in activation of InGaAs photocathode with a higher In composition.

The experimental quantum efficiency curves of the two samples are shown in Fig. 7. In contrast to the theoretical quantum efficiency curves in Fig. 3(a), the experimental quantum efficiency curves follow the trend of the curves obtained by the theoretical model. It can be seen that these experimental quantum efficiency curves have no obvious

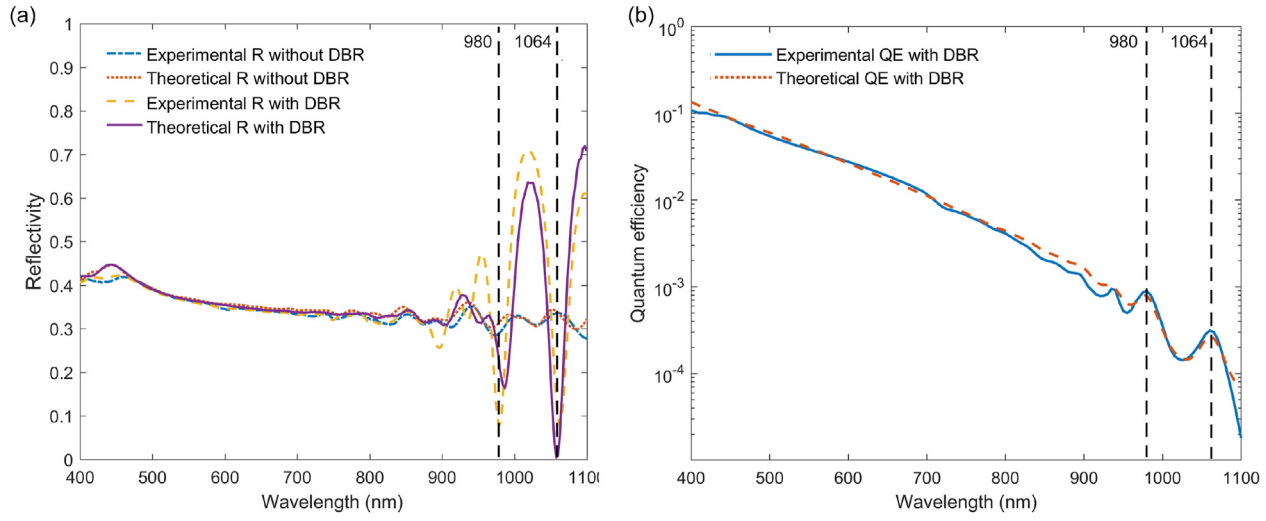

Fig. 6 – (a) Reflectivity curves and (b) quantum efficiency curves of the grown laminated GaAs-based cathode sample.

Table 2 – Fitted performance parameters of the quantum efficiency curves.

Parameter	Value	Description
P_0	0.09	Surface electron escape probability
K	10	Surface potential barrier factor
S_{v5}	10^5 cm/s	Electron recombination at the interface between GaAs and $In_{0.05}Ga_{0.95}As$
$S_{v2\sim4}$	10^4 cm/s	Electron recombination at the inner interfaces in graded bandgap region
S_{v1}	10^3 cm/s	Electron recombination at the interface between graded bandgap region and uniform composition region

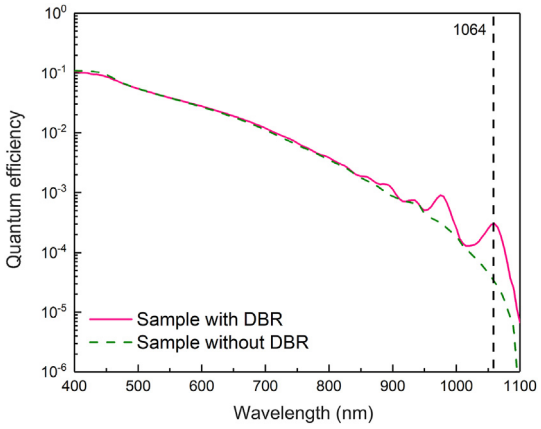

Fig. 7 – Comparison of experimental quantum efficiency curve between the samples with and without DBR layer.

difference in the wavelength range from 400 nm to 850 nm, as predicted before. According to experimental result, the quantum efficiency of the sample with DBR structure can reach 0.0263% at 1064 nm, while the quantum efficiency of the sample without DBR structure is 0.0027% at 1064 nm. The experimental quantum efficiency of the sample with DBR is ten times than that of sample without DBR. The quantum efficiency of the sample with DBR structure can reach 0.0905% at 980 nm, while the quantum efficiency of the sample without DBR structure is 0.0311% at 980 nm. Considering that the activation process of the two samples are consistent, the enhancement of quantum efficiency at 1064 nm and 980 nm can be attributed to the introduction of DBR layer. Through comparison experiments, it is indicated that the graded-bandgap laminated GaAs-based photocathode structure can practically realize the enhancement of the quantum efficiency in the near-infrared range, especially at 1064 nm and 980 nm. However, the experimental quantum efficiency results of the samples are limited by the material growth technology of InGaAs and still have much room for improvement in the further.

5. Conclusion

In summary, a laminated reflection-mode GaAs-based photocathode with a varying-composition emission layer and a DBR structure is proposed for enhancing the quantum efficiency at 1064 nm. The theoretical quantum efficiency and reflectivity spectrum have been simulated by one-dimensional continuity equations and FDTD method, respectively. According to the simulated absorptivity curves and quantum efficiency curves, it is found that the DBR layer effectively increases the absorption ability of emission layer at 1064 nm and consequently enhances the quantum efficiency at 1064 nm. Furthermore, the corresponding GaAs-based cathode samples with the designed structures were prepared for verifying the theoretical prediction and the practicability of the deduced model. The experimental results show that, the proposed photocathode structure can realize the minimum reflectivity at 1064 nm and the quantum efficiency is enhanced by nearly ten times. Finally, a laminated GaAs-based photocathode sample with a quantum efficiency of 0.0263% at 1064 nm was obtained, which is 10 times larger than that of the sample without DBR layer. This structural design concept would provide a method to realize the enhancement of quantum efficiency of reflection-mode photocathode at a specific wavelength, and the quantum efficiency model would provide reliable theoretical guidance for superior photocathodes. After improving the growth quality of InGaAs materials in the future, this new structure will be more critical for improving the quantum efficiency of photocathodes.

Declaration of Competing Interest

The authors declare that they have no known competing financial interests or personal relationships that could have appeared to influence the work reported in this paper.

Acknowledgments

The project was supported by National Natural Science Foundation of China (grant Nos. 61771245 and U2141239); Science and Technology on Low-Light-Level Night Vision Laboratory Foundation of China (J20200102).

REFERENCES

[1] Kaneko H, Minegishi T, Higashi T, Nakabayashi M, Shibata N, Domen K. Stable hydrogen production from water on an NIR-responsive photocathode under harsh conditions. Small 2018;2:1800018.
[2] Zhang Y, Yu YQ, Mi LF, Wang H, Zhu ZF, Wu QY, et al. In situ fabrication of vertical multilayered MoS_2/Si homotype

heterojunction for high-speed visible-near-infrared photodetectors. Small 2016;12:1062–71.
[3] Ye L, Li H, Chen ZF, Xu JB. Near-infrared photodetector based on MoS_2/black phosphorus heterojunction. ACS Photonics 2016;3:692–9.
[4] Chen GH, Yu YQ, Zheng K, Ding T, Wang WL, Jiang Y, et al. Fabrication of ultrathin Bi_2S_3 nanosheets for high-performance, flexible, visible-NIR photodetectors. Small 2015;11:2848–55.
[5] Miao JS, Hu WD, Guo N, Lu ZY, Liu XQ, Liao L, et al. High-responsivity graphene/InAs nanowire heterojunction near-infrared photodetectors with distinct photocurrent on/off ratios. Small 2015;11:936–42.
[6] Dömer H, Bostanjoglo O. High-speed transmission electron microscopy. Rev Sci Instrum 2003;74:4369–72.
[7] Blacksberg J, Maruyama Y, Charbon E, Rossman GR. Fast single-photon avalanche diode arrays for laser Raman spectroscopy. Opt Lett 2011;36:3672–4.
[8] Schwede JW, Sarmiento T, Narasimhan VK, Rosenthal SJ, Riley DC, Schmitt F, et al. Photon-enhanced thermionic emission from heterostructures with low interface recombination. Nat Commun 2013;4:1576.
[9] Wang GY, Chang BK, Yang MJ, Wang K, Tran HC, Liu J, et al. Thermally enhanced photoelectric emission of reflection-mode GaAs photocathode. Sol Energy 2018;174:352–8.
[10] Xiao G, Zheng GH, Qiu M, Li Q, Li DS, Ni MJ. Thermionic energy conversion for concentrating solar power. Appl Energy 2017;208:1318–42.
[11] Karkare S, Boulet L, Cultrera L, Dunham B, Liu XH, Schaff W, et al. Ultrabright and ultrafast III-V semiconductor photocathodes. Phys Rev Lett 2014;112. 097601.
[12] Smirnov KJ, Davydov VV, Glagolev SF, Rodygina NS, Ivanova NV. Photocathodes for near infrared range devices based on InP/InGaAs heterostructures. J Phys: Conf Ser 2018;1038. 012102.
[13] Kildemo M, Maria J, Ellingsen PG, Aas LMS. Parametric model of the Mueller matrix of a Spectralon white reflectance standard deduced by polar decomposition techniques. Opt Express 2013;21:18509–24.
[14] Restelli A, Bienfang JC, Migdall AL. Single-photon detection efficiency up to 50% at 1310 nm with an InGaAs/InP avalanche diode gated at 1.25 GHz. Appl Phys Lett 2013;102:141104.
[15] Yang MZ, Jin MC. Photoemission of reflection-mode InGaAs photocathodes after Cs,O activation and recaesiations. Opt Mater 2016;62:499–504.
[16] Sachno V, Dolgyh A, Loctionov V. Image intensifier tube (I2) with 1.06-μm InGaAs-photocathode. Proc SPIE 2005;5834:169–75.
[17] Bourree LE, Chasse DR, Stephan PL, Glosser R. MBE grown InGaAs photocathode. Proc SPIE 2003;4796:1–10.
[18] Jin MC, Chen XL, Hao GH, Chang BK, Cheng HC. Research on quantum efficiency for reflection-mode InGaAs photocathodes with thin emission layer. Appl Opt 2015;54:8332–8.
[19] Fisher DG, Enstrom RE, Williams BF. Long-wavelength photoemission from $Ga_{1-x}In_xAs$ alloys. Appl Phys Lett 1971;18:371–3.
[20] Spicer WE. Photoemissive, photoconductive, and optical absorption studies of alkali-antimony compounds. Phys Rev 1958;112:114–22.
[21] Fisher DG. The effect of Cs-O activation temperature on the surface escape probability of NEA (In,Ga)As photocathodes. IEEE Trans Electron Dev 1974;21:541–2.
[22] Zou J, Cockayne DJH, Usher BF. Misfit dislocations and critical thickness in InGaAs/GaAs heterostructure systems. J Appl Phys 1993;73:619–26.
[23] Kim HS. Method of fabricating a transmission mode InGaAs photocathode for night vision system. U.S. patent; 1995. p. 5378640. US5378640 A.
[24] Saka T, Kato T, Nakanishi T, Tsubata M, Kishino K, Horinaka H, et al. New-type photocathode for polarized electron source with distributed Bragg reflector. Jpn J Appl Phys 1993;32:1837–40.
[25] Liu W, Chen YQ, Lu WT, Moy A, Poelker M, Stutzman M, et al. Record-level quantum efficiency from a high polarization strained GaAs/GaAsP superlattice photocathode with distributed Bragg reflector. Appl Phys Lett 2016;109:252104.
[26] Grobli JC, Oberli D, Meier F, Dommann A, Mamaev Y, Subashiev A, et al. Polarization resonances of optically spin-oriented photoelectrons emitted from strained semiconductor photocathodes. Phys Rev Lett 1995;74:2106–9.
[27] Yang Y, Yang WZ, Sun CD. Heterostructured cathode with graded bandgap window-layer for photon-enhanced thermionic emission solar energy converters. Sol Energy Mater Sol Cells 2015;132:410–7.
[28] Konagai M, Takahashi K. Graded-band-gap $pGa_{1-x}Al_xAs$-nGaAs heterojunction solar cells. J Appl Phys 1975;46:3542–6.
[29] Feng C, Zhang YJ, Qian YS, Xu Y, Liu XX, Jiao GC. Quantum efficiency of transmission-mode $Al_xGa_{1-x}As$/GaAs photocathodes with graded-composition and exponential-doping structure. Opt Commun 2016;369:50–5.
[30] Zhang YJ, Niu J, Zhao J, Zou JJ, Chang BK, Shi F, et al. Influence of exponential-doping structure on photoemission capability of transmission-mode GaAs photocathodes. J Appl Phys 2010;109. 093108.
[31] Zhang YJ, Chang BK, Niu J, Zhao J, Zou JJ, Shi F, et al. High-efficiency graded band-gap $Al_xGa_{1-x}As$/GaAs photocathodes grown by metalorganic chemical vapor deposition. Appl Phys Lett 2011;99:101104.
[32] Jin MC, Chang BK, Cheng HC, Zhao J, Yang MJ, Chen XL, et al. Research on quantum efficiency of transmission-mode InGaAs photocathode. Optik 2014;125:2395–9.
[33] Wang ZH, Zhang YJ, Qian YS, Li SM, Zhang KM, Shi F, et al. UV-Vis-NIR broadband response of GaAs-based photocathode with multilayer graded-band cascade structure. Superlattice Microst 2021;156:106957.
[34] Feng C, Zhang YJ, Qian YS, Chang BK, Shi F, Jiao GC, et al. Photoemission from advanced heterostructured $Al_xGa_{1-x}As$/GaAs photocathodes under multilevel built-in electric field. Opt Express 2015;23:19478–88.
[35] Levinshtein M, Shur MS, Rumyanstev S. Handbook series on semiconductor parameters. World Scientific; 1996.
[36] Zou JJ, Chang BK, Chen HL, Liu L. Variation of quantum-yield curves for GaAs photocathodes under illumination. J Appl Phys 2007;101. 033126.
[37] Zhang YJ, Zou JJ, Niu J, Zhao J, Chang BK. Photoemission characteristics of different-structure reflection-mode GaAs photocathodes. J Appl Phys 2011;110. 063113.
[38] Aspnes DE, Kelso SM, Logan RA, Bhat R. Optical properties of $Al_xGa_{1-x}As$. J Appl Phys 1986;60:754–67.
[39] http://www.ioffe.ru/SVA/NSM/nk/index.html.